Simultaneous Approximation Terms for Elastic Wave Equations on Nonuniform Grids

Longfei Gao and David Keyes

1 Introduction

Numerical simulation of wave phenomena is routinely used in seismic studies, where simulated wave signals are compared against experimental ones to infer subterranean information. Various wave systems can be used to model wave propagation in earth media. Here, we consider the system of isotropic elastic wave equations described in Section 2. Various numerical methods can be applied to discretize such a system, among which the finite difference methods (FDMs) are still very popular, particularly for seismic exploration applications, due to their simplicity and efficiency.

However, when discretized on uniform grids, heterogeneity of the earth media will lead to oversampling in both space and time, undermining the efficiency of FDMs. Specifically, since spatial grid spacing is usually decided on a point-per-wavelength basis for wave simulations, uniform grid discretization will lead to oversampling in space for regions with higher wave-speeds. On the other hand, temporal step length is usually restricted by the Courant-Friedrichs-Lewy (CFL) stability condition for wave simulations using explicit time stepping methods, which will lead to oversampling in time for regions with lower wave-speeds.

For earth media, the wave-speeds tend to increase with depth due to sedimentation and consolidation. Contrast between the smallest and largest wave-speeds in earth media can be as high as fifty, cf. [1, p. 240], which entails significant oversampling for discretizations on uniform grids. These observations motivate us to consider the grid configuration illustrated in Figure 1, where two uniform grid regions are separated by a horizontal interface. The staggered grid discretization approach, which dates back to [12], is considered here, where different solution variables are discretized on different subgrids. In Figure 1, ratio of the grid spacings of the two regions is two. However, other ratios, not necessarily integers, can also be addressed with the

Longfei Gao & David Keyes
Division of Computer, Electrical and Mathematical Sciences and Engineering,
King Abdullah University of Science and Technology, Thuwal 23955-6900, Saudi Arabia
e-mail: longfei.gao@kaust.edu.sa & david.keyes@kaust.edu.sa

methodology presented here. Furthermore, multiple grid layers can be combined together in a cascading manner to account for larger wave-speed contrasts.

In this work, we recap one of the earliest motivations of domain decomposition methods by demonstrating how to combine the two regions illustrated in Figure 1 without numerical artifacts. Specifically, we adopt the summation by parts (SBP) - simultaneous approximation terms (SATs) approach, which utilizes discrete energy analysis to guide the discretization. The overall semi-discretization is shown to be discretely energy conserving, preserving the analogous property in the continuous elastic wave system. The concept of SBP operators dates back to [7] while the technique of SATs was introduced in [2]. The two review papers [11, 3] provide comprehensive coverage of their developments. While the 2D elastic wave system is considered here to demonstrate the methodology, we expect the presented procedure to extend straightforwardly to the 3D case.

In the following, we describe the abstracted mathematical problem in Section 2, present the interface treatment in Section 3, provide numerical examples in Section 4, and summarize in Section 5.

2 Problem Description

We consider the 2D isotropic elastic wave equations posed as the following first-order dynamical system written in terms of velocity and stress:

$$\begin{cases} \dfrac{\partial v_x}{\partial t} = \dfrac{1}{\rho}\left(\dfrac{\partial \sigma_{xx}}{\partial x} + \dfrac{\partial \sigma_{xy}}{\partial y}\right); \\ \dfrac{\partial v_y}{\partial t} = \dfrac{1}{\rho}\left(\dfrac{\partial \sigma_{xy}}{\partial x} + \dfrac{\partial \sigma_{yy}}{\partial y}\right); \\ \dfrac{\partial \sigma_{xx}}{\partial t} = (\lambda + 2\mu)\dfrac{\partial v_x}{\partial x} + \lambda \dfrac{\partial v_y}{\partial y} + \mathcal{S}; \\ \dfrac{\partial \sigma_{xy}}{\partial t} = \mu \dfrac{\partial v_y}{\partial x} + \mu \dfrac{\partial v_x}{\partial y}; \\ \dfrac{\partial \sigma_{yy}}{\partial t} = \lambda \dfrac{\partial v_x}{\partial x} + (\lambda + 2\mu)\dfrac{\partial v_y}{\partial y} + \mathcal{S}, \end{cases} \tag{1}$$

where v_x and v_y are particle velocities; σ_{xx}, σ_{xy} and σ_{yy} are stress components; ρ, λ and μ are density, first and second Lamé parameters that characterize the medium; $\mathcal{S}$ is the source term that drives the wave propagation. Lamé parameters λ and μ are related with the compressional and shear wave-speeds c_p and c_s through $\lambda = \rho(c_p^2 - 2c_s^2)$ and $\mu = \rho c_s^2$. For simplicity, the source term $\mathcal{S}$ is omitted in the upcoming discussion. All solution variables and their derivatives are assumed to be zero at the initial time. We consider periodic boundary condition for left and right boundaries and free-surface boundary condition for top and bottom boundaries.

The above system is equivalent to system (2), which is more natural for energy analysis and derivation of the interface treatment. In (2), the Einstein summation convention applies to subscript indices k and l. Coefficients s_{xxkl}, s_{xykl} and s_{yykl} are components of the compliance tensor, which can be expressed in terms of λ and μ. However, their exact expressions are not needed for the upcoming discussion. As

explained later in Section 3, system (1) is still the one used for implementation.

$$\begin{cases} \rho \dfrac{\partial v_x}{\partial t} = \dfrac{\partial \sigma_{xx}}{\partial x} + \dfrac{\partial \sigma_{xy}}{\partial y}; \\ \rho \dfrac{\partial v_y}{\partial t} = \dfrac{\partial \sigma_{xy}}{\partial x} + \dfrac{\partial \sigma_{yy}}{\partial y}; \\ s_{xxkl} \dfrac{\partial \sigma_{kl}}{\partial t} = \dfrac{\partial v_x}{\partial x}; \\ s_{xykl} \dfrac{\partial \sigma_{kl}}{\partial t} = \dfrac{1}{2}\left(\dfrac{\partial v_y}{\partial x} + \dfrac{\partial v_x}{\partial y}\right); \\ s_{yykl} \dfrac{\partial \sigma_{kl}}{\partial t} = \dfrac{\partial v_y}{\partial y}. \end{cases} \tag{2}$$

The staggered grids illustrated in Figure 1 are used to discretize the above systems, where two uniform grid regions are separated by a horizontal interface, with a contrast ratio 1 : 2 in grid spacing. Both regions include the interface in discretization.

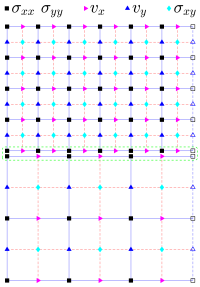

Fig. 1: Illustration of the grid configuration.

3 Methodology

In this section, we demonstrate how to couple the discretizations of system (1) on the two uniform grid regions illustrated in Figure 1 using the SBP-SAT approach. A similar work has been presented in [4] for acoustic wave equations. We will follow the methodology and terminology developed therein.

The continuous energy associated with system (2), and system (1) by equivalence, can be expressed as:

$$e = \int_\Omega \tfrac{1}{2} \rho v_i v_i d_\Omega + \int_\Omega \tfrac{1}{2} \sigma_{ij} s_{ijkl} \sigma_{kl} d_\Omega \,, \tag{3}$$

where Ω denotes a simply connected domain; the Einstein summation convention applies to subscript indices i, j, k and l. The two integrals of (3) correspond to the kinetic and potential parts of the continuous energy, respectively. Differentiating e with respect to time t and substituting the equations from (2), it can be shown that

$$\frac{de}{dt} = \int_{\partial\Omega} v_i \sigma_{ij} n_j d_{\partial\Omega}, \tag{4}$$

where $\partial\Omega$ denotes the boundary of Ω. For the free-surface boundary condition, i.e., $\sigma_{ij} n_j = 0$, and periodic boundary condition considered in this work, we have $de/dt = 0$, i.e., system (2) conserves energy e.

Spatially discretizing (2) with finite difference methods on a uniform grid leads to the following semi-discretized system:

$$\begin{cases} \mathcal{A}^{V_x}\boldsymbol{\rho}^{V_x}\dfrac{dV_x}{dt} = \mathcal{A}^{V_x}\mathcal{D}_x^{\Sigma_{xx}}\Sigma_{xx} + \mathcal{A}^{V_x}\mathcal{D}_y^{\Sigma_{xy}}\Sigma_{xy}; \\ \mathcal{A}^{V_y}\boldsymbol{\rho}^{V_y}\dfrac{dV_y}{dt} = \mathcal{A}^{V_y}\mathcal{D}_x^{\Sigma_{xy}}\Sigma_{xy} + \mathcal{A}^{V_y}\mathcal{D}_y^{\Sigma_{yy}}\Sigma_{yy}; \\ \mathcal{A}^{\Sigma_{xx}}S_{xxkl}^{\Sigma_{kl}}\dfrac{d\Sigma_{kl}}{dt} = \mathcal{A}^{\Sigma_{xx}}\mathcal{D}_x^{V_x}V_x; \\ \mathcal{A}^{\Sigma_{xy}}S_{xykl}^{\Sigma_{kl}}\dfrac{d\Sigma_{kl}}{dt} = \frac{1}{2}\mathcal{A}^{\Sigma_{xy}}\left(\mathcal{D}_x^{V_y}V_y + \mathcal{D}_y^{V_x}V_x\right); \\ \mathcal{A}^{\Sigma_{yy}}S_{yykl}^{\Sigma_{kl}}\dfrac{d\Sigma_{kl}}{dt} = \mathcal{A}^{\Sigma_{yy}}\mathcal{D}_y^{V_y}V_y, \end{cases} \tag{5}$$

where the Einstein summation convention applies only to k and l in the subscripts, but not to those appearing in the superscripts. Superscript such as ^{V_x} indicates the grid with which the underlying quantity or operator is associated. In (5), $\mathcal{D}$ symbolizes a finite difference matrix, while $\mathcal{A}$ symbolizes a diagonal norm matrix with its diagonal component loosely representing the area that the corresponding grid point occupies. From the implementation perspective, the norm matrices in (5) are redundant, but they will play an important role in deriving the proper interface treatment. These 2D finite difference matrices and norm matrices are constructed from their 1D counterparts via tensor product. Specifically,

$$\begin{aligned} &\mathcal{A}^{V_x} = \mathcal{A}_x^M \otimes \mathcal{A}_y^N, \quad \mathcal{A}^{V_y} = \mathcal{A}_x^N \otimes \mathcal{A}_y^M, \\ &\mathcal{A}^{\Sigma_{xy}} = \mathcal{A}_x^M \otimes \mathcal{A}_y^M, \ \mathcal{A}^{\Sigma_{xx}} = \mathcal{A}^{\Sigma_{yy}} = \mathcal{A}_x^N \otimes \mathcal{A}_y^N, \end{aligned} \tag{6}$$

and

$$\begin{aligned} &\mathcal{D}_x^{V_x} = \mathcal{D}_x^M \otimes \mathcal{I}_y^N, \quad \mathcal{D}_x^{V_y} = \mathcal{D}_x^N \otimes \mathcal{I}_y^M, \quad \mathcal{D}_x^{\Sigma_{xy}} = \mathcal{D}_x^M \otimes \mathcal{I}_y^M, \quad \mathcal{D}_x^{\Sigma_{xx}} = \mathcal{D}_x^N \otimes \mathcal{I}_y^N, \\ &\mathcal{D}_y^{V_x} = \mathcal{I}_x^M \otimes \mathcal{D}_y^N, \quad \mathcal{D}_y^{V_y} = \mathcal{I}_x^N \otimes \mathcal{D}_y^M, \quad \mathcal{D}_y^{\Sigma_{xy}} = \mathcal{I}_x^M \otimes \mathcal{D}_y^M, \quad \mathcal{D}_y^{\Sigma_{yy}} = \mathcal{I}_x^N \otimes \mathcal{D}_y^N, \end{aligned} \tag{7}$$

where $\mathcal{I}$ symbolizes a 1D identity matrix. Superscript ^{N} indicates the '*normal*' grid that aligns with the boundaries while ^{M} indicates the '*modified*' grid that is staggered with respect to the '*normal*' grid. The specific forms of the 1D norm matrices and 1D finite difference matrices in (6) and (7) have been described in [5, p. 672][1]. By construction, they satisfy the following relations:

$$\mathcal{A}_x^N\mathcal{D}_x^M + \left(\mathcal{A}_x^M\mathcal{D}_x^N\right)^T = \mathbf{0}\,; \tag{8a}$$

$$\mathcal{A}_y^N\mathcal{D}_y^M + \left(\mathcal{A}_y^M\mathcal{D}_y^N\right)^T = \mathcal{E}_y^R\left(\mathcal{P}_y^R\right)^T - \mathcal{E}_y^L\left(\mathcal{P}_y^L\right)^T, \tag{8b}$$

where $\mathcal{E}_y^R$ and $\mathcal{E}_y^L$ are canonical basis vectors that select values of the solution variables defined on the N grid at the top and bottom boundaries, respectively, while $\mathcal{P}_y^R$ and $\mathcal{P}_y^L$ are projection vectors that extrapolate values of the solution variables defined on the M grid to the top and bottom boundaries, respectively.

The discrete energy associated with semi-discretized system (5) is defined as:

$$E = \frac{1}{2}V_i^T\left(\mathcal{A}^{V_i}\boldsymbol{\rho}^{V_i}\right)V_i + \frac{1}{2}\Sigma_{ij}^T\left(\mathcal{A}^{\Sigma_{ij}}S_{ijkl}^{\Sigma_{kl}}\right)\Sigma_{kl}\,, \tag{9}$$

where, as in (5), the Einstein summation convention applies only to i, j, k, and l in the subscripts. Differentiating E with respect to time t and substituting the equations

[1] We use this specific set of operators here to demonstrate the methodology, while alternative choices exist (e.g., [9]), for which the presented methodology can still be applied with minor modifications.

from (5), it can be shown that

$$\begin{aligned}\frac{dE}{dt} &= V_x^T \left[I_x^M \otimes \mathcal{E}_y^R\right] \mathcal{A}_x^M \left[I_x^M \otimes (\mathcal{P}_y^R)^T\right] \Sigma_{xy} + \Sigma_{yy}^T \left[I_x^N \otimes \mathcal{E}_y^R\right] \mathcal{A}_x^N \left[I_x^N \otimes (\mathcal{P}_y^R)^T\right] V_y \\ &\quad - V_x^T \left[I_x^M \otimes \mathcal{E}_y^L\right] \mathcal{A}_x^M \left[I_x^M \otimes (\mathcal{P}_y^L)^T\right] \Sigma_{xy} - \Sigma_{yy}^T \left[I_x^N \otimes \mathcal{E}_y^L\right] \mathcal{A}_x^N \left[I_x^N \otimes (\mathcal{P}_y^L)^T\right] V_y ,\end{aligned} \tag{10}$$

where the first two terms are associated with the top boundary while the last two terms are associated with the bottom boundary, as indicated by the respective selection and projection operators appearing in these terms. With the above discrete energy analysis result, we can now modify system (5) accordingly to account for boundary and interface conditions.

In the following, we use superscripts $^+$ and $^-$ to distinguish systems or terms from the upper and lower regions of Figure 1, respectively. To account for the free-surface boundary condition on the top boundary, i.e., $\sigma_{xy} = \sigma_{yy} = 0$, the first two equations in the upper region system are appended with penalty terms, i.e., SATs, as follows:

$$(+)\begin{cases} \mathcal{A}^{V_x^+} \boldsymbol{\rho}^{V_x^+} \dfrac{dV_x^+}{dt} = \mathcal{A}^{V_x^+} \mathcal{D}_x^{\Sigma_{xx}^+} \Sigma_{xx}^+ + \mathcal{A}^{V_x^+} \mathcal{D}_y^{\Sigma_{xy}^+} \Sigma_{xy}^+ \\ \qquad\qquad + \eta_T^{V_x^+} \left[I_x^{M^+} \otimes \mathcal{E}_y^{R^+}\right] \mathcal{A}_x^{M^+} \left\{\left[I_x^{M^+} \otimes (\mathcal{P}_y^{R^+})^T\right] \Sigma_{xy}^+ - \mathbf{0}\right\}; \\ \mathcal{A}^{V_y^+} \boldsymbol{\rho}^{V_y^+} \dfrac{dV_y^+}{dt} = \mathcal{A}^{V_y^+} \mathcal{D}_x^{\Sigma_{xy}^+} \Sigma_{xy}^+ + \mathcal{A}^{V_y^+} \mathcal{D}_y^{\Sigma_{yy}^+} \Sigma_{yy}^+ \\ \qquad\qquad + \eta_T^{V_y^+} \left[I_x^{N^+} \otimes \mathcal{P}_y^{R^+}\right] \mathcal{A}_x^{N^+} \left\{\left[I_x^{N^+} \otimes (\mathcal{E}_y^{R^+})^T\right] \Sigma_{yy}^+ - \mathbf{0}\right\}, \end{cases} \tag{11}$$

where $\eta_T^{V_x^+} = \eta_T^{V_y^+} = -1$ are penalty parameters. The forms of the penalty terms and values of the penalty parameters are chosen so that the energy-conserving property from the continuous system is preserved. To see this, we differentiate E from (9) with respect to time t as before. After substitution, the penalty terms in (11) bring two extra terms into dE/dt, i.e.,

$$\eta_T^{V_x^+} (V_x^+)^T \left[I_x^{M^+} \otimes \mathcal{E}_y^{R^+}\right] \mathcal{A}_x^{M^+} \left[I_x^{M^+} \otimes (\mathcal{P}_y^{R^+})^T\right] \Sigma_{xy}^+$$

and

$$\eta_T^{V_y^+} (V_y^+)^T \left[I_x^{N^+} \otimes \mathcal{P}_y^{R^+}\right] \mathcal{A}_x^{N^+} \left[I_x^{N^+} \otimes (\mathcal{E}_y^{R^+})^T\right] \Sigma_{yy}^+.$$

By setting $\eta_T^{V_x^+} = \eta_T^{V_y^+} = -1$, these extra terms cancel out the first two terms in (10), which are associated with the top boundary. Similar modifications presented later in (12)-(14) are obtained by following the same procedure and rationale. It is worth mentioning that such procedure and rationale for deriving the proper boundary and interface treatment, particularly the usage of the energy method, is very similar to that for flux specification in discontinuous Galerkin methods, cf., for example, [6].

Similarly, to account for the free-surface boundary condition on the bottom boundary, the first two equations of the lower region system are modified as follows:

$$(-)\begin{cases} \mathcal{A}^{V_x^-} \boldsymbol{\rho}^{V_x^-} \dfrac{dV_x^-}{dt} = \mathcal{A}^{V_x^-} \mathcal{D}_x^{\Sigma_{xx}^-} \Sigma_{xx}^- + \mathcal{A}^{V_x^-} \mathcal{D}_y^{\Sigma_{xy}^-} \Sigma_{xy}^- \\ \qquad\qquad + \eta_B^{V_x^-} \left[I_x^{M^-} \otimes \mathcal{E}_y^{L^-}\right] \mathcal{A}_x^{M^-} \left\{\left[I_x^{M^-} \otimes (\mathcal{P}_y^{L^-})^T\right] \Sigma_{xy}^- - \mathbf{0}\right\}; \\ \mathcal{A}^{V_y^-} \boldsymbol{\rho}^{V_y^-} \dfrac{dV_y^-}{dt} = \mathcal{A}^{V_y^-} \mathcal{D}_x^{\Sigma_{xy}^-} \Sigma_{xy}^- + \mathcal{A}^{V_y^-} \mathcal{D}_y^{\Sigma_{yy}^-} \Sigma_{yy}^- \\ \qquad\qquad + \eta_B^{V_y^-} \left[I_x^{N^-} \otimes \mathcal{P}_y^{L^-}\right] \mathcal{A}_x^{N^-} \left\{\left[I_x^{N^-} \otimes (\mathcal{E}_y^{L^-})^T\right] \Sigma_{yy}^- - \mathbf{0}\right\}, \end{cases} \tag{12}$$

where $\eta_B^{V_x^-} = \eta_B^{V_y^-} = 1$ are the chosen penalty parameters.

To account for the interface conditions (cf. [10, p. 52]), i.e., $\sigma^+_{xy}=\sigma^-_{xy}$, $\sigma^+_{yy}=\sigma^-_{yy}$, $v^+_x=v^-_x$, and $v^+_y=v^-_y$, the upper and lower region systems are further modified by appending additional SATs as follows:

$$
(+)\begin{cases}
\mathcal{A}^{V^+_x}\boldsymbol{\rho}^{V^+_x}\dfrac{dV^+_x}{dt}=\mathcal{A}^{V^+_x}\mathcal{D}^{\Sigma^+_{xx}}_x\Sigma^+_{xx}+\mathcal{A}^{V^+_x}\mathcal{D}^{\Sigma^+_{xy}}_y\Sigma^+_{xy}\\
\quad+\eta_I^{V^+_x}\left[\mathcal{I}^{M^+}_x\otimes\mathcal{E}^{L^+}_y\right]\mathcal{A}^{M^+}_x\left\{\left[\mathcal{I}^{M^+}_x\otimes(\mathcal{P}^{L^+}_y)^T\right]\Sigma^+_{xy}-\mathcal{T}^{M^+_-}\left(\left[\mathcal{I}^{M^-}_x\otimes(\mathcal{P}^{R^-}_y)^T\right]\Sigma^-_{xy}\right)\right\};\\
\mathcal{A}^{V^+_y}\boldsymbol{\rho}^{V^+_y}\dfrac{dV^+_y}{dt}=\mathcal{A}^{V^+_y}\mathcal{D}^{\Sigma^+_{xy}}_x\Sigma^+_{xy}+\mathcal{A}^{V^+_y}\mathcal{D}^{\Sigma^+_{yy}}_y\Sigma^+_{yy}\\
\quad+\eta_I^{V^+_y}\left[\mathcal{I}^{N^+}_x\otimes\mathcal{P}^{L^+}_y\right]\mathcal{A}^{N^+}_x\left\{\left[\mathcal{I}^{N^+}_x\otimes(\mathcal{E}^{L^+}_y)^T\right]\Sigma^+_{yy}-\mathcal{T}^{N^+_-}\left(\left[\mathcal{I}^{N^-}_x\otimes(\mathcal{E}^{R^-}_y)^T\right]\Sigma^-_{yy}\right)\right\};\\
\mathcal{A}^{\Sigma^+_{xx}}S^{\Sigma^+_{kl}}_{xxkl}\dfrac{d\Sigma^+_{kl}}{dt}=\mathcal{A}^{\Sigma^+_{xx}}\mathcal{D}^{V^+_x}_xV^+_x;\\
\mathcal{A}^{\Sigma^+_{xy}}S^{\Sigma^+_{kl}}_{xykl}\dfrac{d\Sigma^+_{kl}}{dt}=\frac{1}{2}\mathcal{A}^{\Sigma^+_{xy}}\left(\mathcal{D}^{V^+_y}_xV^+_y+\mathcal{D}^{V^+_x}_yV^+_x\right)\\
\quad+\frac{1}{2}\eta_I^{\Sigma^+_{xy}}\left[\mathcal{I}^{M^+}_x\otimes\mathcal{P}^{L^+}_y\right]\mathcal{A}^{M^+}_x\left\{\left[\mathcal{I}^{M^+}_x\otimes(\mathcal{E}^{L^+}_y)^T\right]V^+_x-\mathcal{T}^{M^+_-}\left(\left[\mathcal{I}^{M^-}_x\otimes(\mathcal{E}^{R^-}_y)^T\right]V^-_x\right)\right\};\\
\mathcal{A}^{\Sigma^+_{yy}}S^{\Sigma^+_{kl}}_{yykl}\dfrac{d\Sigma^+_{kl}}{dt}=\mathcal{A}^{\Sigma^+_{yy}}\mathcal{D}^{V^+_y}_yV^+_y\\
\quad+\eta_I^{\Sigma^+_{yy}}\left[\mathcal{I}^{N^+}_x\otimes\mathcal{E}^{L^+}_y\right]\mathcal{A}^{N^+}_x\left\{\left[\mathcal{I}^{N^+}_x\otimes(\mathcal{P}^{L^+}_y)^T\right]V^+_y-\mathcal{T}^{N^+_-}\left(\left[\mathcal{I}^{N^-}_x\otimes(\mathcal{P}^{R^-}_y)^T\right]V^-_y\right)\right\},
\end{cases}
\tag{13}
$$

$$
(-)\begin{cases}
\mathcal{A}^{V^-_x}\boldsymbol{\rho}^{V^-_x}\dfrac{dV^-_x}{dt}=\mathcal{A}^{V^-_x}\mathcal{D}^{\Sigma^-_{xx}}_x\Sigma^-_{xx}+\mathcal{A}^{V^-_x}\mathcal{D}^{\Sigma^-_{xy}}_y\Sigma^-_{xy}\\
\quad+\eta_I^{V^-_x}\left[\mathcal{I}^{M^-}_x\otimes\mathcal{E}^{R^-}_y\right]\mathcal{A}^{M^-}_x\left\{\left[\mathcal{I}^{M^-}_x\otimes(\mathcal{P}^{R^-}_y)^T\right]\Sigma^-_{xy}-\mathcal{T}^{M^-_+}\left(\left[\mathcal{I}^{M^+}_x\otimes(\mathcal{P}^{L^+}_y)^T\right]\Sigma^+_{xy}\right)\right\};\\
\mathcal{A}^{V^-_y}\boldsymbol{\rho}^{V^-_y}\dfrac{dV^-_y}{dt}=\mathcal{A}^{V^-_y}\mathcal{D}^{\Sigma^-_{xy}}_x\Sigma^-_{xy}+\mathcal{A}^{V^-_y}\mathcal{D}^{\Sigma^-_{yy}}_y\Sigma^-_{yy}\\
\quad+\eta_I^{V^-_y}\left[\mathcal{I}^{N^-}_x\otimes\mathcal{P}^{R^-}_y\right]\mathcal{A}^{N^-}_x\left\{\left[\mathcal{I}^{N^-}_x\otimes(\mathcal{E}^{R^-}_y)^T\right]\Sigma^-_{yy}-\mathcal{T}^{N^-_+}\left(\left[\mathcal{I}^{N^+}_x\otimes(\mathcal{E}^{L^+}_y)^T\right]\Sigma^+_{yy}\right)\right\};\\
\mathcal{A}^{\Sigma^-_{xx}}S^{\Sigma^-_{kl}}_{xxkl}\dfrac{d\Sigma^-_{kl}}{dt}=\mathcal{A}^{\Sigma^-_{xx}}\mathcal{D}^{V^-_x}_xV^-_x;\\
\mathcal{A}^{\Sigma^-_{xy}}S^{\Sigma^-_{kl}}_{xykl}\dfrac{d\Sigma^-_{kl}}{dt}=\frac{1}{2}\mathcal{A}^{\Sigma^-_{xy}}\left(\mathcal{D}^{V^-_y}_xV^-_y+\mathcal{D}^{V^-_x}_yV^-_x\right)\\
\quad+\frac{1}{2}\eta_I^{\Sigma^-_{xy}}\left[\mathcal{I}^{M^-}_x\otimes\mathcal{P}^{R^-}_y\right]\mathcal{A}^{M^-}_x\left\{\left[\mathcal{I}^{M^-}_x\otimes(\mathcal{E}^{R^-}_y)^T\right]V^-_x-\mathcal{T}^{M^-_+}\left(\left[\mathcal{I}^{M^+}_x\otimes(\mathcal{E}^{L^+}_y)^T\right]V^+_x\right)\right\};\\
\mathcal{A}^{\Sigma^-_{yy}}S^{\Sigma^-_{kl}}_{yykl}\dfrac{d\Sigma^-_{kl}}{dt}=\mathcal{A}^{\Sigma^-_{yy}}\mathcal{D}^{V^-_y}_yV^-_y\\
\quad+\eta_I^{\Sigma^-_{yy}}\left[\mathcal{I}^{N^-}_x\otimes\mathcal{E}^{R^-}_y\right]\mathcal{A}^{N^-}_x\left\{\left[\mathcal{I}^{N^-}_x\otimes(\mathcal{P}^{R^-}_y)^T\right]V^-_y-\mathcal{T}^{N^-_+}\left(\left[\mathcal{I}^{N^+}_x\otimes(\mathcal{P}^{L^+}_y)^T\right]V^+_y\right)\right\},
\end{cases}
\tag{14}
$$

where $\eta_I^{V^+_x}=\eta_I^{\Sigma^+_{xy}}=\eta_I^{V^+_y}=\eta_I^{\Sigma^+_{yy}}=\frac{1}{2}$ and $\eta_I^{V^-_x}=\eta_I^{\Sigma^-_{xy}}=\eta_I^{V^-_y}=\eta_I^{\Sigma^-_{yy}}=-\frac{1}{2}$ are the chosen penalty parameters. Moreover, $\mathcal{T}^{M^+_-}$, $\mathcal{T}^{N^+_-}$ in (13) and $\mathcal{T}^{M^-_+}$, $\mathcal{T}^{N^-_+}$ in (14) are interpolation operators that satisfy the following relations:

$$
\mathcal{A}^{N^+}_x\mathcal{T}^{N^+_-}=\left(\mathcal{A}^{N^-}_x\mathcal{T}^{N^-_+}\right)^T\ \text{ and }\ \mathcal{A}^{M^+}_x\mathcal{T}^{M^+_-}=\left(\mathcal{A}^{M^-}_x\mathcal{T}^{M^-_+}\right)^T.
\tag{15}
$$

They operate on the interface only, e.g., $\mathcal{T}^{N^+_-}$ interpolates from lower region N grid points on the interface to upper region N grid points on the interface. Their derivations are usually assisted by symbolic computing software. For the interface illustrated in Figure 1, which has a 1 : 2 contrast in grid spacing, the operators $\mathcal{T}^{N^+_-}$ and $\mathcal{T}^{M^+_-}$ that we use here are characterized by the formulas in (16) and (17), respectively, for the collections of grid points illustrated in Figure 2; moreover, $\mathcal{T}^{N^-_+}$ and $\mathcal{T}^{M^-_+}$ can be derived from $\mathcal{T}^{N^+_-}$ and $\mathcal{T}^{M^+_-}$, respectively, via the relations in (15).

As in the case of SBP operators, these interpolation operators are not unique, either.

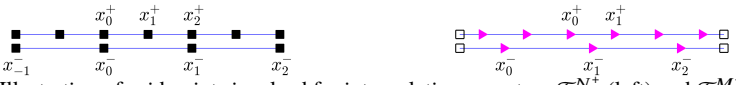

Fig. 2: Illustration of grid points involved for interpolation operators $\mathcal{T}^{\mathcal{N}_-^+}$ (left) and $\mathcal{T}^{\mathcal{M}_-^+}$ (right).

$$f(x_0^+) \leftarrow f(x_0^-);\ f(x_1^+) \leftarrow -\tfrac{1}{16}f(x_{-1}^-)+\tfrac{9}{16}f(x_0^-)+\tfrac{9}{16}f(x_1^-)-\tfrac{1}{16}f(x_2^-);\ f(x_2^+) \leftarrow f(x_1^-). \tag{16}$$

$$f(x_0^+) \leftarrow \tfrac{5}{32}f(x_0^-)+\tfrac{15}{16}f(x_1^-)-\tfrac{3}{32}f(x_2^-); \qquad f(x_1^+) \leftarrow -\tfrac{3}{32}f(x_0^-)+\tfrac{15}{16}f(x_1^-)+\tfrac{5}{32}f(x_2^-). \tag{17}$$

With the above choices on the SATs, it can be verified that the overall semi-discretization conserves the discrete energy E from (9). Now that the proper SATs have been derived, we can remove the norm matrices by dividing them from both sides of the equations in (11-14). From the implementation perspective, the appended SATs amount to modifying the corresponding derivative approximations, e.g., the SAT in the first equation of (14) modifies $\mathcal{D}_y^{\Sigma_{xy}^-}\Sigma_{xy}^-$. Written in terms of these modified derivative approximations, the above discretizations for system (2) can be easily reverted to forms that conform to system (1).

4 Numerical examples

The first example concerns a homogeneous medium characterized by parameters $\rho = 1\,\mathrm{kg/m^3}$, $c_p = 2\,\mathrm{m/s}$ and $c_s = 1\,\mathrm{m/s}$. The grid spacings of the upper and lower regions are chosen as 0.004 m and 0.008 m, respectively, while the time step length is chosen as 0.001 s, which is ~ 0.707 of the CFL limit associated with an infinite uniform grid with 0.004 m grid spacing. The rest of the numerical setup is the same as that for the first example of [4, p. 435], including sizes of the grids, source and receiver locations, and source profile.

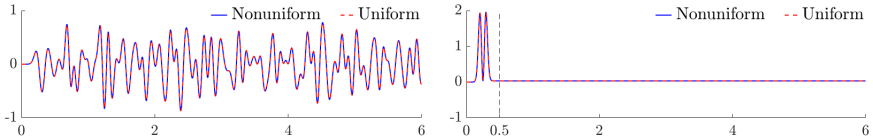

Fig. 3: Seismogram (left) and evolvement of discrete energy (right); Homogeneous media.

The recorded seismogram and evolvement of discrete energy for the first 6 s are displayed in Figure 3, where we observe good agreement between the uniform grid simulation result and the nonuniform grid simulation result using the presented SBP-SAT approach. The source term $\mathcal{S}$, cf. (1), which is omitted from the analysis, is responsible for the initial '*bumps*' in the evolvement of discrete energy. After the source effect tapers off at around 0.5 s (cf. [5, p. 684]), the discrete energy remains constant as expected (at a value ~ 0.0318).

The second example concerns a heterogeneous medium downsampled from the Marmousi2 model, cf. [8]. Wave-speeds c_p and c_s are illustrated in Figure 4.[2] Grid spacing is chosen as 2 m and 4 m for upper and lower regions (separated by the

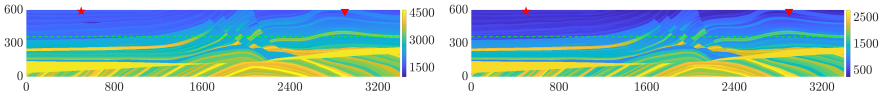

Fig. 4: Media parameters c_p (left) and c_s (right); Colorbar reflects wave-speed with unit m/s.

green dashed line), respectively. Time step length is chosen as 2e-4 s and 3e-4 s for uniform and nonuniform grid simulations, respectively. Same plots as in the previous example are displayed in Figure 5, from where similar observations can be made.

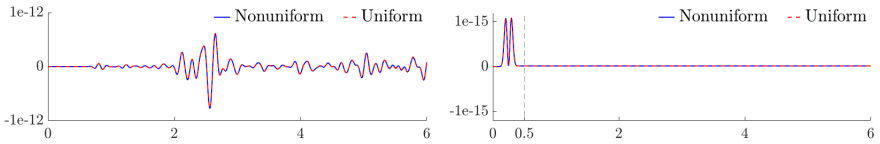

Fig. 5: Seismogram (left) and evolvement of discrete energy (right); Heterogeneous media.

In this example, the ratio between the numbers of spatial grid points in uniform and nonuniform grid simulations is ∼1.813. As a rough estimation, the amount of arithmetic operations per time step is assumed to be linearly proportional to the number of spatial grid points. We therefore expect the ratio between runtimes to be ∼2.719, with an extra factor of 1.5 coming from the difference in total time steps. A test with our Matlab code reveals a ratio of ∼2.681 in runtimes (average of 5 runs), which agrees well with the above complexity analysis result.

5 Summary

Finite difference discretization of the isotropic elastic wave system is considered. An interface treatment procedure is presented to connect two uniformly discretized regions with different grid spacings. The interface conditions are weakly imposed through carefully designed simultaneous approximation terms. The overall semi-discretization conserves a discrete energy that resembles the continuous physical energy, which is demonstrated on both homogeneous and heterogeneous media.

Acknowledgements Gao and Keyes gratefully acknowledge the support of KAUST's OSR under CCF-CAF/URF/1-2596. The authors would also like to thank KSL for computing resources. Part of this work was conducted while the first author was visiting IPAM (Sep - Dec 2018).

[2] To simplify the discussion, the distance between neighboring parameter grid points is assigned to 2 m, which is the same as the grid spacing used in uniform grid simulation. Bilinear interpolation is used when discretization grid points do not match parameter grid points due to grid staggering. We note here that media parameters for uniform grid and nonuniform grid simulations are sampled differently; thus, small discrepancies in simulation results should be allowed.

References

1. Bourbié, T., Coussy, O., Zinszner, B.: Acoustics of Porous Media. Institut Français du Pétrole Publications. Editions Technip (1987)
2. Carpenter, M.H., Gottlieb, D., Abarbanel, S.: Time-stable boundary conditions for finite-difference schemes solving hyperbolic systems: methodology and application to high-order compact schemes. J. Comput. Phys. **111**(2), 220–236 (1994). DOI:10.1006/jcph.1994.1057
3. Del Rey Fernández, D.C., Hicken, J.E., Zingg, D.W.: Review of summation-by-parts operators with simultaneous approximation terms for the numerical solution of partial differential equations. Comput. & Fluids **95**, 171–196 (2014). DOI:10.1016/j.compfluid.2014.02.016
4. Gao, L., Del Rey Fernández, D.C., Carpenter, M., Keyes, D.: SBP-SAT finite difference discretization of acoustic wave equations on staggered block-wise uniform grids. J. Comput. Appl. Math. **348**, 421–444 (2019). DOI:10.1016/j.cam.2018.08.040
5. Gao, L., Keyes, D.: Combining finite element and finite difference methods for isotropic elastic wave simulations in an energy-conserving manner. J. Comput. Phys. **378**, 665–685 (2019). DOI:10.1016/j.jcp.2018.11.031
6. Hesthaven, J.S., Warburton, T.: Nodal discontinuous Galerkin methods, *Texts in Applied Mathematics*, vol. 54. Springer, New York (2008). DOI:10.1007/978-0-387-72067-8. Algorithms, analysis, and applications
7. Kreiss, H.O., Scherer, G.: Finite element and finite difference methods for hyperbolic partial differential equations. In: Mathematical aspects of finite elements in partial differential equations. Academic Press (1974)
8. Martin, G.S., Wiley, R., Marfurt, K.J.: Marmousi2: An elastic upgrade for marmousi. The Leading Edge **25**(2), 156–166 (2006)
9. O'Reilly, O., Lundquist, T., Dunham, E.M., Nordström, J.: Energy stable and high-order-accurate finite difference methods on staggered grids. J. Comput. Phys. **346**, 572–589 (2017). DOI:10.1016/j.jcp.2017.06.030
10. Stein, S., Wysession, M.: An introduction to seismology, earthquakes, and earth structure. John Wiley & Sons (2009)
11. Svärd, M., Nordström, J.: Review of summation-by-parts schemes for initial-boundary-value problems. J. Comput. Phys. **268**, 17–38 (2014). DOI:10.1016/j.jcp.2014.02.031
12. Yee, K.: Numerical solution of initial boundary value problems involving maxwell's equations in isotropic media. IEEE Transactions on antennas and propagation **14**(3), 302–307 (1966)